Applied Catalysis B: Environmental 231 (2018) 262–268

Contents lists available at ScienceDirect

Applied Catalysis B: Environmental

journal homepage: www.elsevier.com/locate/apcatb

Catalytic hydrodehalogenation over supported gold: Electron transfer versus hydride transfer

Yuanyuan Wang[a,b], Qian Zhu[a,b], Yan Wei[a,b], Yanjun Gong[a,b], Chuncheng Chen[a,b], Wenjing Song[a,b,*], Jincai Zhao[a,b]

[a] Key Laboratory of Photochemistry, CAS Research/Education Center for Excellence in Molecular Sciences, Institute of Chemistry, Chinese Academy of Sciences, Beijing, 100190, PR China
[b] University of Chinese Academy of Sciences, Beijing, 100049, PR China

ARTICLE INFO

Keywords:
Selective hydrodehalogenation
Photocatalysis
Supported gold
Electron transfer
Hydride transfer

ABSTRACT

Selective hydrodehalogenation of a variety of aromatic halides (e.g., halogen subsitute phenones and hexafluorobenzene) using isopropanol as the hydrogen source was successfully achieved over supported Au nanoparticles. Distinct reaction pathways were established based on kinetic analysis and intermediate identification. Surface hydrides generated by isopropanol oxidation mediate the hydrodehalogenation by nucleophilic attack without the involvement of carbon centered radical. On the other hand, engeretic electrons on Au nanoparticles populated by visible light irradiation trigger the dissciation of carbon halogen bond (C—X) by injection to the substrates' lowest unoccupied molecular orbitals (LUMO). The super-linear dependency on light intensity, shape of the action spectrum and formation of aryl radical revealed that electron transfer dominates the hydrodehalogneation process, which features a significantly lower activation barrier than transfer of surface hydride. The observed activity is correlated to energy levels of the substrate electron accepting states.

1. Indroduction

Catalytic hydrodehalogenation using an alcohol as the hydrogen source [1–5] has drawn great attention in recent years as a safe and green alternative to H_2 activation under high temperature and high pressure [6,7]. Successful hydrogenation of halogenated organics have been demonstrated with supported metal nanostructures (e.g., Pd, Rh, Pt, Cu, or metallic alloys [2,4,8–10]), holding great promise for the detoxification of contaminants of this class, as well as the synthesis of important intermediates for pharmaceuticals. In analogue to the reaction using H_2 as the hydrogen source, hydrogen species (H atom or hydride) that accumulate upon dehydrogenation of alcohol at metal surfaces are proposed to be active for hydrodehalogenation, via nucleophilic addition or substitution [11]. Supported Pd and Rh on TiO_2 were shown to be most active in catalyzing hydrogenation of chlorobenzene under UV irradiation [8]. In supported Pt-Pd alloy, density of hydrides on Pd surface can be boosted by accepting excited Pt electron, leading to enhanced conversion efficiency of chlorobenzene under visible irradiation [12]. In alternative, heterolysis of the C—X bond can be achieved by single electron transfer [5,13–15]. Efficient separation of photo-generated electrons and holes is the key to successful photocatalytic reactions via electron transfer (e.g., oxygen activation and CO_2 reduction), which can be achieved by constructing heterojunctions from multiple components with suitable energy band, as well as light absorption [16–20]. Recently, we developed TiO_2/Cu hybrid catalyst for debromination of decabromodiphenyl ether (BDE209), where copper nanoparticles not only facilitate charge separation but also mediate the inner-sphere electron transfer to BDE209 to break the C—Br bond. Moreover, the SPR effect of copper creates more energetic electrons and promotes the electron transfer induced hydrodebromination under simultaneous UV and visible irradiation [9].

Despite the great progresses in the development of metal nanomaterial based catalysts, the mechanistic scenario for hydrodehalogenation on metal surfaces has not been well established. In general, hydrogen/hydride transfer is preferred on metals with low hydrogen overpotentials (e.g., Pd and Rh) [8]. For metals featuring intermediate overpotential values(e.g., Cu, Au, and Ni) [21], both hydride and electron transfer are operable with different contributions in hydrodehalogenation which may be tuned by external stimuli (e.g., temperature, irradiation wavelength, electrochemical potential or surface coordinating ligands) [21–23]. Also the chemo- or regio- selectivity are dependences of reaction pathway due to the distinct transition state and

* Corresponding author at: Key Laboratory of Photochemistry, CAS Research/Education Center for Excellence in Molecular Sciences, Institute of Chemistry, Chinese Academy of Sciences, Beijing, 100190, PR China.
E-mail address: wsongunc@iccas.ac.cn (W. Song).

https://doi.org/10.1016/j.apcatb.2018.03.032
Received 17 January 2018; Received in revised form 26 February 2018; Accepted 9 March 2018
Available online 10 March 2018
0926-3373/

reaction barrier [24,25]. Revealing the reaction mechanism and their operating conditions would guide the design of metal based catalytic system for targeting substrates.

Gold nanostructures are actively involved in catalytic selective oxidation, coupling reaction as well as hydrogenation of carbon dioxide and various organic functionalities [20,22,26–38]. The property and catalytic performance of gold are highly tunable by morphology, size and support [33,34,37]. However, catalytic hydrodehalogenation with gold based catalysts has rarely been demonstrated. Gold itself services as catalyst for both alcohol oxidation and the subsequent hydrogenation via hydride or electron transfer. Surface hydrogen species generate during alcohol oxidation are reported to act as hydrogen donor of 2,2′-6,6′-tetramethylpiperidine N-oxyl (TEMPO) and 5,5-dimethyl-1-pyrroline N-oxide (DMPO) on CeO_2 supported Au nanoparticles [39–41]. Electron transfer was proposed to contribute to the light driven hydrogenation of cinnamon aldehyde by isopropanol on SiC supported Au [42]. Hydrogenation via energetic electron transfer to substrates was also supported by a correlation of wavelength threshold and reduction potentials of various functionalities (epoxide, carbonyl and nitro groups) [22,43].

As part of our continuous effort to develop efficient catalyst for hydrodehalogenation of aromatic halides, the catalytic activity/selectivity of supported gold was explored and the operating pathways are elucidated by dependency of hydrogenation kinetics on temperature, light intensity/wavelength, as well as intermediates identification. TiO_2 (anatase) supported Au nanoparticles show excellent performance for hydrogenation of a large scope of aromatic halides (e.g., 4′-bromoacetophenone and hexafluorobenzene) with high selectivity towards carbon halogen bond under visible light irradiation. While both electron transfer and hydride transfer are operable on Au nanostructures, a super-linear light intensity dependency and action spectrum indicate the major contribution of direct electron transfer to halogenated substrate to break the carbon halogen bond. Hydrodehalogenation via nucleophilic attack by surface hydride plays less significant role but its relative contribution increases at higher temperature. For aryl halides investigated here, electron transfer features significantly lower activation barrier and is kinetically faster in comparison to hydride transfer. The activities and reaction scope are also in line with electron transfer thermodynamics.

2. Experimental section

2.1. Chemicals and materials

Anatase TiO_2 (99.7%, 240 m^2/g), CeO_2 (99.9%), tetrachloroauric (III) acid trihydrate (99.99%), sodium borohydride (98%), potassium hydroxide (99.98%), TEMPO (98%) and α-bromostyrene (95%) were purchased from Acros Organics. ZrO_2 (< 100 nm) was purchased from Aldrich. 4′-Bromoacetophenone (98%), 4′-bromopropiophenone (97%), 4′-iodoacetophenone (98%), 4-bromostyrene (98%), 4-bromophenylacetylene (97%) and propiophenone (99%) were purchased from Alfa Aesar. 4-Bromobenzophenone (98%) was purchased from Innochem. Bromobenzene (99%), 9-bromoanthracene, 1, 3-dibromo-5-fluorobenzene (98%), acetophenone (98%), hexafluorobenzene (98%), styrene (99.5%), pyrrole (99%) and N-methylpyrrole (99%) were purchased from J&K. 2, 2′, 4, 4′-tetrabromodiphenyl ether (> 95%) was purchased from Ark. Isopropanol (99.9%) used throughout this study was of high-performance liquid chromatography (HPLC) grade (Dikma Technologies, ON, Canada). All the chemicals were used as received without further purification.

2.2. Catalysts preparation

Au (3 wt%) on TiO_2 was synthesized by a photodeposition method. Briefly, 1 g of titanium dioxide powder was suspended in a mixture of 60 ml of water and 10 ml of isopropanol. A certain amount of an aqueous tetrachloroauric acid (30 mg Au) solution was gradually added to the above suspension under argon. Then the suspension was exposed to a 300 W xenon lamp (PLS-SXE-300/300UV) equipped with a 300 nm long path filter and an infrared filter under continuous stirring. The color of the suspension gradually turned purple. After 2 h of irradiation, the purple precipitate was separated by centrifugation and washed with deionized water three times. Finally, the obtained product was dried at 60 °C for 24 h in a vacuum oven. The dry powder was then calcined at 450 °C for 30 min. Au (3 wt%) on TiO_2, CeO_2, ZrO_2 and layered double hydroxide (LDH) was prepared by $NaBH_4$ reduction, as reported elsewhere [44].

2.3. Characterization of the catalysts

X-ray diffraction (XRD) patterns of the as-prepared catalysts was obtained on an X-ray diffractometer (Rigaku, Japan) using Cu Kα radiation at a scan sate of 5° min^{-1}. Typical high-angle annular dark-field scanning transmission electron microscopy (HAADF-STEM) and HR-TEM images were taken on a JEM-2100F electron microscope (JEOL, Japan) with a 200 kV accelerating voltage. The UV–vis diffuse-reflectance spectra were obtained on a SHIMADZU UV-2600 spectrophotometer. XPS measurements were performed on an ESCALAB 250XI electron spectrometer with a Mg Kα (1253.6 eV) source. All binding energies were referenced to the C 1s peak at 284.8 eV from adventitious carbon.

2.4. Catalytic hydrodehalogenation

All reactions were conducted under an argon atmosphere unless otherwise noted. Typically, 1 μmol substrate was dissolved into 9 ml of isopropanol in a pyrex vessel. Then, 1 ml of a 0.1 M KOH solution in isopropanol and 50 mg of 3 wt% Au/TiO_2 were added into the mixture. The vessel was purged with argon for 20 min to remove O_2, and the reaction system was saturated with argon during the irradiation. The suspensions were stirred by a magnetic stirrer during reaction with or without irradiation ($\lambda > 420$ nm) provided by a Xe lamp. The temperature range was from 298 to 343 K in either conditions. The suspension (1 ml) was collected at given irradiation time intervals and centrifuged immediately at 10000 rpm for 10 min to remove the Au/TiO_2 particles. The supernatants were analysed by an Agilent 1260 HPLC or an Agilent 7890B GC as detailed in the Supporting Information.

To probe the role of surface hydrides, conversion of 4′-bromoacetophenone was monitored with 50 equivalents of pyrrole to block the surface Lewis base sites on Au/TiO_2. The products were monitored by HPLC.

The aryl radicals generated during hydrogenation were trapped by N-methylpyrrole (100-fold in excess) under photocatalytic or thermocatalytic condition. The products were monitored by HPLC.

3. Results and discussion

3.1. Characterization of supported Au nanoparticles

Supported gold nanoparticles were prepared photochemically in isopropanol/water mixed solvent (on anatase TiO_2) or using $NaBH_4$ as chemical reductant [44] (on TiO_2, ZrO_2, CeO_2 and LDH as detailed in experimental section. Homogenous distribution of gold nanospheres (~20 nm) was observed for the photochemically prepared Au/TiO_2 by the high-angle annular dark-field scanning transmission electron microscopy and EDX mapping (Fig. 1a–e). The lattice fringes of 0.204 nm was resolved by high-resolution transmission electron microscopy (HR-TEM, Fig. 1f), which is consistent with Au (200) facet in the XRD spectrum (PDF number: 4–784) as shown in Fig. S1. The binding energy at 83.2 and 86.9 eV for Au $4f_{7/2}$ and Au $4f_{5/2}$ confirmed the metallic state (Fig. 1g). 2–5 nm Au particles supported on TiO_2, CeO_2, ZrO_2 or

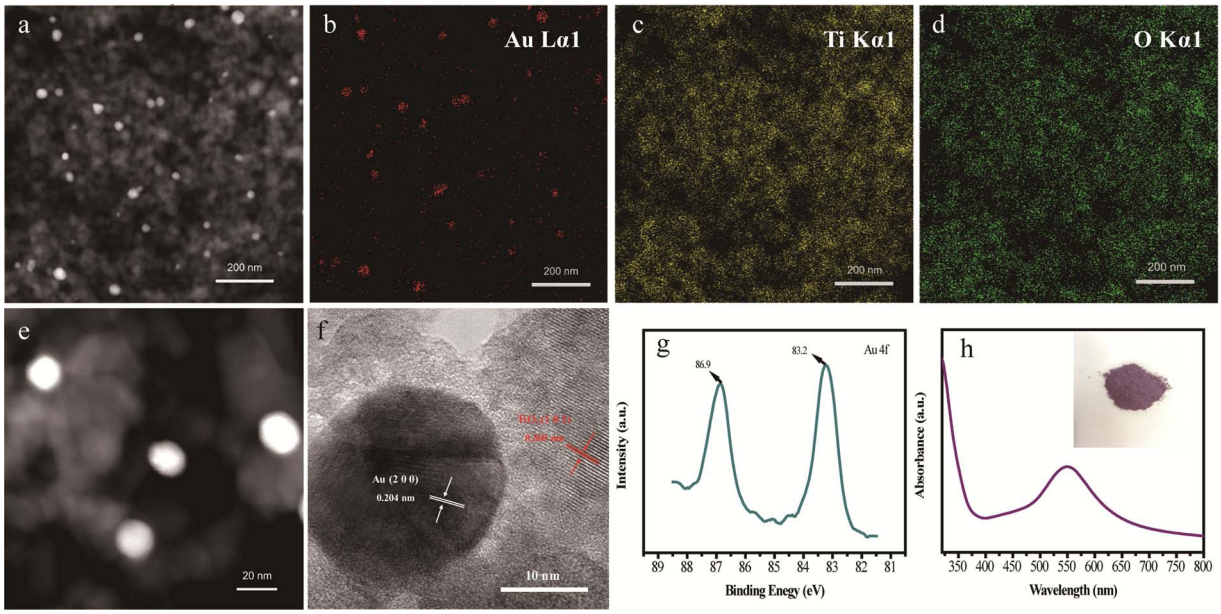

Fig. 1. Characterizations of Au/TiO_2. (a)-(e) HAADF-STEM images and EDX mapping spectra for Au, Ti and O; (f) HR-TEM image; (g) XPS showing the Au ($4f_{7/2,\ 5/2}$) peaks; (h) UV–vis diffuse-reflectance spectrum of Au/TiO_2 powder.

LDH was obtained by chemical reduction (Fig. S2). The as-prepared samples are deep purple exhibiting the characteristic SPR absorption of gold nanospheres around 550 nm (Fig. 1h).

3.2. Performance of supported Au in hydrodehalogenation

An activity survey was conducted using 4′-bromoacetophenone (0.1 mM) as the model compound in isopropanol with 0.01 M KOH. Photochemically prepared Au/TiO_2 (3 wt%) sample demonstrated the best catalytic performance under visible light irradiation above 420 nm and can be reused without the loss in activity for multiple runs (Fig. S3). 96% conversion of 4′-bromoacetophenone completes in 1 h, quantitatively producing acetophenone (99% selectivity) and Br^- (Table 1, entry 1 and Fig. 2). No side reactions (e.g., hydrogen evolution) was observed during the reaction. When using TiO_2 supported gold prepared by chemical reduction, the catalytic activity dropped to 93% where small amount of 1-(4-bromophenyl)ethanol was produced (Fig. S4); Other substrates supported Au samples (on CeO_2, ZrO_2 and LDH) also catalyzed the hydrodebromination but the activity was 2–3 times lower comparing to that of Au/TiO_2 (Table S1).

A variety of aryl halides can be effectively converted to hydrogenated products with Au/TiO_2 prepared by the photo-reduction as summarized in Table 1. The thermocatalytic conversion for selected substrates is also provided. For substrates with additional reducible groups (4′-bromoacetophenone, 4′-bromopropiophenone, 4′-iodoacetophenone, 4-bromobenzophenone, 9-bromoanthracene and α-bromostyrene, entries 1–6), excellent selectivity for hydrodehalogenation was observed (ketone, vinyl groups and anthracene skeleton remained intact). Polyhalogenated aromatic compounds such as hexafluorobenzene, 2, 2′, 4, 4′-tetrabromodiphenyl ether, 1, 3, 5-tribromobenzene, 1, 3-dibromo-5-chlorobenzene and 1, 3-dibromo-5-fluorobenzene also underwent dehalogenation with over 85% selectivity. But the activity was limited and the reaction stops as lower-halogenated congeners; Dehalogenation of bromobenzene, 4-bromostyrene and 4-bromophenylacetylene cannot be accomplished on Au/TiO_2. The selectivity and activity will be discussed in detail considering the operable reaction pathways under different conditions.

3.3. Hydrodehalogenation pathways

The reaction process was monitored to identify the operable dehalogenation pathway. It was noted that acetone was produced before irradiation (Supporting information, Fig. S5a), consistent with the Au-catalyzed dehydrogenation of isopropanol, forming surface hydride species (Au-H) [41] as the reducing equivalents. Generation of ~4 mM acetone from isopropanol oxidation was observed within 20 min, significantly faster than the rate of hydrodebromination and was not affected by the presence of substrate (Fig. S5). According to the amount of oxidized isopropanol, Au-H species is in large excess. As a nucleophile, surface hydride species could attacks to the neighboring carbon atom of C—X bond (Scheme 1 top, nucleophilic addition). In another proposed mechanism, hydride attack the carbon atom of C—X (nucleophilic substitution) [11]. At 298 K, however, reaction with Au-H only accounts for 7% conversion of 4′-bromoacetophenone without visible irradiation (Fig. S5b); The rate of hydrodebromination increased at elevated temperature: conversion of 90% of 4′-bromoacetophenone to acetophenone (98% selectivity) can be achieved within an hour at 323 K (Table 1, entry 1). The critical role of surface hydride species in the reaction was supported by the termination of hydrodebromination in the presence of pyrrole (50 equivalent), a typical blocker of surface Lewis base sites (Fig. S6) [45]. Conversion of hexafluorobenzene via hydride transfer was also explored under thermocatalytic condition. It was note that despite a complete depletion of substrate after 12 h of reaction at 323 K, the yield of pentafluorobenzene was only 2.3%, significantly lower than 43% obtained in photocatalytic reaction (Table 1 entry 7). The difference in reaction kinetics as well as product selectivity suggests that alternative reaction pathway prevails and contributes to the activity under visible irradiation. It is worth to mention that under the light intensity used here (400 mW cm^{-2}), the temperature increase by non-radiative decay of hot electrons is expected to be less than 1 K [43], which exclude the photo-thermal driven hydrodehalogenation (via hydride transfer).

The kinetics of visible light driven hydrodebromination was investigated at different irradiation intensities (0.1–0.4 W cm^{-2}, Fig. S7). As depicted in Fig. 3a, the conversion rate show a super-linear dependency on the irradiation intensity ($R \propto I^n$, n = 2, 298 K), which is a signature feature of electron transfer mediated reaction by metal nanostructures [46]. For aryl halides, transfer of the energetic electron to

Table 1
Scope of hydrogenation of organic halides catalyzed by Au/TiO_2.

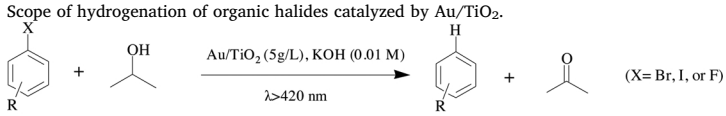

Entry	Substrate	Product	Conv. (%)	Sel. (%)
1	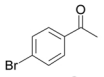		96 (90)	99 (98)
2	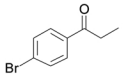		85	98
3	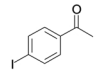		100	99
4	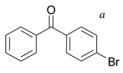	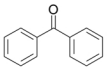	29	98
5	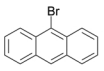	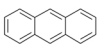	85	99
6			100	98
7			50 (100)	86 (2.3)
8	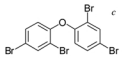	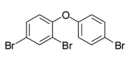	53 (0)	88 (0)
9			54	100
10			78	96
11			86	99

Reaction conditions: 2-PrOH (10 ml), substrate (0.1 mM), KOH (0.01 M), catalyst (50 mg), Ar atmosphere, 1 h reaction under visible-light irradiation (> 420 nm, 0.4 W/cm^2), and at a temperature of 298 K unless otherwise noted. [a] 12 h under visible-light irradiation; [b] Substrate (1 mM), 12 h under visible-light irradiation; [c] Substrate (0.01 mM). The numbers in the brackets represent conversion at 323 K in the dark.

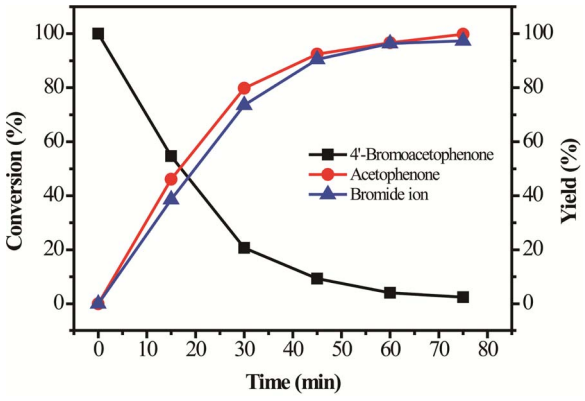

Fig. 2. Temporal profiles of 4′-bromoacetophenone, acetophenone and Br^- during photocatalytic reaction under irradiation above 420 nm (400 mW cm^{-2}).

the π* orbital is the rate limiting step [47], followed by the rapid intramolecular electron transfer to the anti-bonding σ* orbital of C-Br, producing aryl radical and bromide (Scheme 1, bottom). Generation of aryl radical was confirmed by its characteristic coupling reaction with N-methylpyrrole under photocatalytic condition (Fig. S8). In contrast, no coupling products was identified in the hydrodebromination via hydride transfer at 323 K (Fig. S8).

The wavelength dependence of 4′-bromoacetophenone debromination was further investigated. In this experiment, the photon flux at each wavelength (400 nm to 600 nm) was maintained as 3.67×10^{-7} Einstein cm^{-2} s^{-1}, and the action spectrum was directly obtained from the conversion yield (Fig. 3b). Different from the shape of Au SPR absorption spectrum, the action spectrum exhibits a continuous increase from 600 to 400 nm. Such a mismatch can be attributed to the LUMO energy levels of the substrates relative to the Fermi level of Au on TiO_2 [43]: when LUMO level is high in the energy diagram, shorter wavelength photons populates electron to the energy level locates above LUMO of the substrate to drive a thermodynamic favored process. Although concentration of the energetic electrons are expected to be high by irradiation near a wavelength of 550 nm, the electron transfer suffers from a small driving force and/or insufficient overlap of the density of states (DOS) of energetic electrons and the LUMO of 4′-bromoacetophenone. This is in analogous to the Sonogashira coupling over supported Au-Pd with 1-iodo-4-methoxybenzene as the starting material

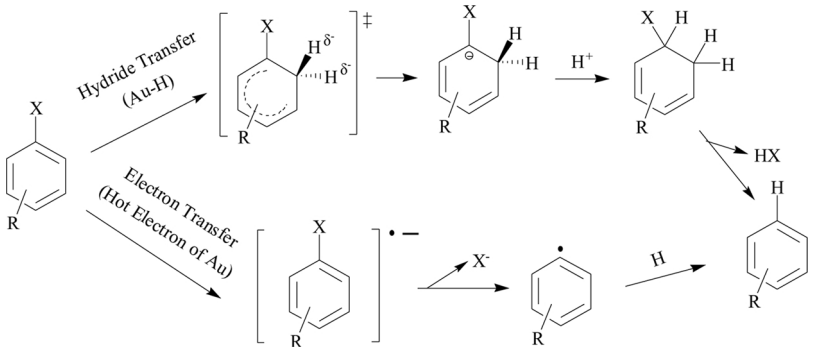

Scheme 1. Reaction Pathways for Hydrodehalogenation Catalyzed by Au/TiO_2.

[43]. The contribution of electron transfer was also supported by the fact that hydrodebromination was not inhibited by pyrrole under visible irradiation (Fig. S9).

Using the temperature dependency of the conversion rate in thermocatalytic and photocatalytic reaction, activation energy of nucleophilic addition of hydride to aryl ring of 4′-bromoacetophenone was calculated to be 98.7 kJ mol^{-1}, whereas electron transfer mediated hydrogenation show a significantly lower barrier, 40.6 kJ mol^{-1} (Fig. 4). Comparing to hydride transfer, light driven electron transfer on Au/TiO_2 is more feasible for hydrodehalogenation. This also applies to the hydrogenation of hexafluorobenzene and 2, 2′, 4, 4′-tetrabromodiphenyl ether as summarized in Table 1. The preference for electron transfer or hydride transfer mediated hydrodehalogenation is a result from thermodynamics and kinetic competition of the two pathways, which depend on the hydrogen overpotentials, nature of surface Au—H bond, energy level of hot carriers and Fermi level. For the aromatic halides tested here, the LUMO generally locate on the aryl π* orbital, electron injection to this orbital rapidly shift to the antibonding σ* orbital to break C—X bond, which is kinetically feasible. Despite hydride transfer is not the dominant pathway under visible irradiation at 298 K, its contribution is expected to increase at higher temperature and may surpass that of electron transfer at certain point (Fig. 4c). It shall also be noted that for metal material with suitable hydrogen adsorption/desorption kinetics, hydride transfer could be dominant as was demonstrated on Pd under UV or visible irradiation [12,48].

In the light driven hydrodebromination, the activity and reaction scope are in line with the electron transfer driving force, i.e., the energy gap between the populated excited electrons and the LUMO of halogenated substrates (generally the π* orbital), the latter of which can be evaluated by reduction potentials [47]. Cyclic voltammogram (CV) of 4′-bromoacetophenone shows two cathodic peaks at −1.5 and −1.8 V vs. Ag/AgCl assigned to the debromination and acetophenone reduction (Fig. S10a, the latter was generated near the working electrode in the first electrochemical process). Therefore, the former is more accessible by photo-excited electrons, and the cleavage of C—Br is triggered by the intramolecular electron transfer from the π* orbital to the antibonding σ* orbital of C—Br bond. Considering a Fermi level of 0.45 eV for Au (the Fermi level alignment with the anatase TiO_2 support was not considered for simplification), excitation by 600 nm photons could generate electrons with sufficient energy to drive C—Br activation, consistent with action spectrum. In addition to halo-phenone derivatives, the efficient photocatalytic hydrodebromination of the structurally distinct 9-bromoanthracene is also achieved ($E_{p,c}$ = −1.5 V, Fig. S10a). The hydrogenation of hexafluorobenzene also proceed but the reaction ceased at pentafluorobenzene, due to the higher LUMO level of the latter (−2.0 and −2.3 V, Fig. S10b). This also applies to other polyhalogenated substrates because low-halogenated congeners have more negative reduction potentials. For bromobenzene, 4-bromostyrene and 4-bromophenylacetylene with values of $E_{p,c}$ more negative than −2.2 V (Fig. S10c), no hydrogenation occurred using Au/TiO_2. The limitation arises from the energy level that can be reached by visible light populated hot electrons; the energy loss in the ultrafast cooling stage further decreases the electron transfer driving force and limits the activity.

Now we turn to the prior selectivity of the present catalytic system towards hydrodehalogenation to ketone moiety in selected substrates. According to CV (Fig. S10), electrochemical reduction of acetophenone via single electron transfer occurs at −1.8 V, which is 300 mV negative than reductive debromination but is more positive than hexafluorobenzene (−2.0 V). A rough estimation show that irradiation above 420 nm is able to trigger an energetic favored electron transfer to phenone derivatives, in contrast to our observation. It is accepted that for acetophenone reduction, single electron transfer is kinetics challenge due to the formation high energy ketyl intermediates. Generally a coupled proton transfer or coordination of ketyl to a transition metal (e.g., Ti^{3+}) could assist the reduction process [49]. On the contrary, the kinetics of debromination via electron transfer is rather feasible due to the rapid C-Br bond breaking (10^7 s^{-1}) of the aryl radical anion intermediates [47,50]. Furthermore, introduction of KOH is known to promote the removal of halide anions for hydrodebromination via both

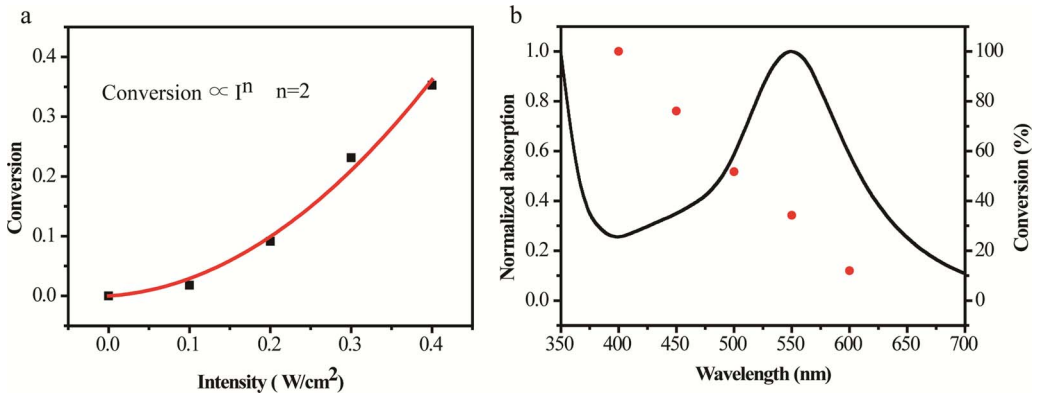

Fig. 3. (a) Conversion of 4′-bromoacetophenone by 10 min irradiation as a function of the light intensity; (b) action spectrum calculated using the conversion obtained at 2 h (dots, right axis) and the absorption spectrum of Au/TiO_2 powder (solid line, left axis) (For interpretation of the references to colour in this figure legend, the reader is referred to the web version of this article).

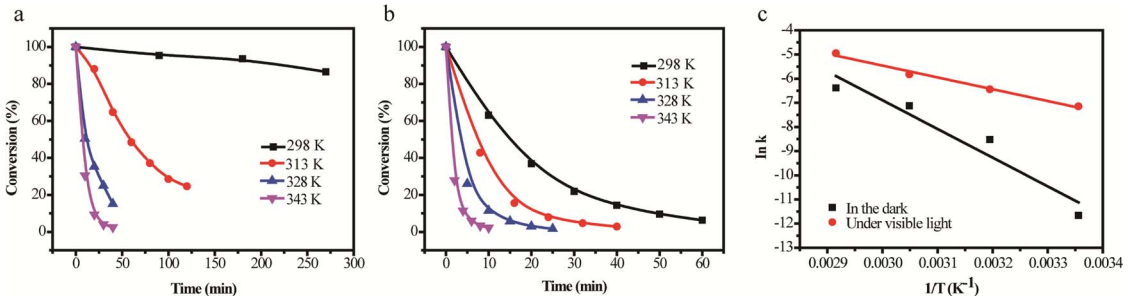

Fig. 4. Temperature dependency the conversion of 4′-bromoacetophenone (a) in the dark or (b) under irradiation above 420 nm; (c) Arrhenius plot of thermocatalytic and photocatalytic hydrodebromination of 4′-bromoacetophenone.

hydride and electron transfer, despite its precise role in the catalytic steps has not been well illustrated. For reduction of ketone, however, addition of base may disfavor the single electron transfer. Indeed, under UV irradiation, where alcohol is oxidized by valence band hole of TiO_2 (base is not required for alcohol oxidation) and electron/proton stored on Au, 4′-bromoacetophenone underwent 100% ketone reduction. In earlier reported Au catalyzed ketone reduction, the base to substrate ratio (1:10) is much less than the condition used here. The significant different interfacial environment, including adsorption of substrate/intermediates and hydroxyl groups, could be responsible for the observed selectivity. This is subjected to further investigation.

4. Conclusion

A simple and sustainable approach for hydrodehalogenation based on TiO_2 supported gold is presented, where efficient and selective hydrogenation of a variety of aromatic halides is achieved under visible irradiation. Dehydrogenation of isopropanol in the presence of base produces Au-H species, which undergoes nucleophilic addition to aryl ring to initiate the hydrodehalogenation. Visible light irradiation populates Au electrons to higher energy level, which are injected into the LUMO of halogenated substrates, breaking C—X bond to give aryl radical and halide anions. The electron transfer mediated activation of carbon halogen bond features a much lower energy barrier, dominating the visible light driven hydrodehalogenation. The observed activities and kinetics are governed by property of surface hydride and electron transfer thermodynamics. An essential role of base in the prior selectivity towards dehalogenation was also highlighted. The mechanistic scenario revealed here could guide the design of catalyst with specific activity towards targeting molecules and reactions.

Acknowledgement

This work was supported by NSFC (Nos. 21590811, 21677148, 21521062, 21525729), the “Strategic Priority Research Program” of the Chinese Academy of Sciences (No. XDA09030200) and the “Key Research Program of Frontier Sciences” (No. QYZDY-SSW-SLH028) of the Chinese Academy of Sciences.

Appendix A. Supplementary data

Supplementary material related to this article can be found, in the online version, at doi:https://doi.org/10.1016/j.apcatb.2018.03.032.

References

[1] C.Y. Sun, D. Zhao, C.C. Chen, W.H. Ma, J.C. Zhao, Environ. Sci. Technol. 43 (2009) 157–162.
[2] L. Li, W. Chang, Y. Wang, H. Ji, C. Chen, W. Ma, J. Zhao, Chem.-Eur. J. 20 (2014) 11163–11170.
[3] M. Lei, N. Wang, L. Zhu, Q. Zhou, G. Nie, H. Tang, Appl. Catal. B-Environ. 182 (2016) 414–423.
[4] E.M. Zahran, N.M. Bedford, M.A. Nguyen, Y.-J. Chang, B.S. Guiton, R.R. Naik, L.G. Bachas, M.R. Knecht, J. Am. Chem. Soc. 136 (2014) 32–35.
[5] Q. Zhu, Y. Wang, H. Zhang, R. Duan, C. Chen, W. Song, J. Zhao, Appl. Catal. B-Environ. 219 (2017) 322–328.
[6] S. De Corte, T. Hennebel, J.P. Fitts, T. Sabbe, V. Biznuk, S. Verschuere, D. van der Lelie, W. Verstraete, N. Boon, Environ. Sci. Technol. 45 (2011) 8506–8513.
[7] M.L. Buil, M.A. Esteruelas, S. Niembro, M. Olivan, L. Orzechowski, C. Pelayo, A. Vallribera, Organometallics 29 (2010) 4375–4383.
[8] K. Fuku, K. Hashimoto, H. Kominami, Chem. Commun. 46 (2010) 5118–5120.
[9] Y. Lv, X. Cao, H. Jiang, W. Song, C. Chen, J. Zhao, Appl. Catal. B-Environ. 194 (2016) 150–156.
[10] Y. Shiraishi, Y. Takeda, Y. Sugano, S. Ichikawa, S. Tanaka, T. Hirai, Chem. Commun. 47 (2011) 7863–7865.
[11] D. Sadowsky, K. McNeill, C.J. Cramer, Environ. Sci. Technol. 48 (2014) 10904–10911.
[12] H. Sakamoto, J. Imai, Y. Shiraishi, S. Tanaka, S. Ichikawa, T. Hirai, Acs. Catal. 7 (2017) 5194–5201.
[13] A.A. Isse, S. Gottardello, C. Durante, A. Gennaro, Phys. Chem. Chem. Phys. 10 (2008) 2409–2416.
[14] Y.-F. Huang, D.-Y. Wu, A. Wang, B. Ren, S. Rondinini, Z.-Q. Tian, C. Amatore, J. Am. Chem. Soc. 132 (2010) 17199–17210.
[15] C. Durante, V. Perazzolo, L. Perini, M. Favaro, G. Granozzi, A. Gennaro, Appl. Catal. B-Environ. 158 (2014) 286–295.
[16] D. Chen, K. Wang, D. Xiang, R. Zong, W. Yao, Y. Zhu, Appl. Catal. B-Environ. 147 (2014) 554–561.
[17] Q. Hao, X. Niu, C. Nie, S. Hao, W. Zou, J. Ge, D. Chen, W. Yao, Phys. Chem. Chem. Phys. 18 (2016) 31410–31418.
[18] G. Yang, D. Chen, H. Ding, J. Feng, J.Z. Zhang, Y. Zhu, S. Hamid, D.W. Bahnemann, Appl. Catal. B-Environ. 219 (2017) 611–618.
[19] Q. Hao, R. Wang, H. Lu, Ca. Xie, W. Ao, D. Chen, C. Ma, W. Yao, Y. Zhu, Appl. Catal. B-Environ. 219 (2017) 63–72.
[20] M.-Y. Xing, B.-X. Yang, H. Yu, B.-Z. Tian, S. Bagwasi, J.-L. Zhang, X.-Q. Gong, J. Phys. Chem. Lett. 4 (2013) 3910–3917.
[21] X.H. Chadderdon, D.J. Chadderdon, J.E. Matthiesen, Y. Qiu, J.M. Carraher, J.-P. Tessonnier, W. Li, J. Am. Chem. Soc. 139 (2017) 14120–14128.
[22] X. Ke, S. Sarina, J. Zhao, X. Zhang, J. Chang, H. Zhu, Chem. Commun. 48 (2012) 3509–3511.
[23] J.L. Fiorio, N. Lopez, L.M. Rossi, Acs. Catal. 7 (2017) 2973–2980.
[24] H. Robatjazi, H. Zhao, D.F. Swearer, N.J. Hogan, L. Zhou, A. Alabastri, M.J. McClain, P. Nordlander, N.J. Halas, Nat.Commun. 8 (2017) 27.
[25] Y. Li, H. Ji, C. Chen, W. Ma, J. Zhao, Angew. Chem. Int. Ed. 52 (2013) 12636–12640.
[26] W. Tu, Y. Zhou, H. Li, P. Li, Z. Zou, Nanoscale 7 (2015) 14232–14236.
[27] J.A. Trindell, J. Clausmeyer, R.M. Crooks, J. Am. Chem. Soc. 139 (2017) 16161–16167.
[28] Y. Fang, J.C. Flake, J. Am. Chem. Soc. 139 (2017) 3399–3405.
[29] H. Zhu, X. Ke, X. Yang, S. Sarina, H. Liu, Angew. Chem. Int. Ed. 49 (2010) 9657–9661.
[30] A. Tanaka, K. Fuku, T. Nishi, K. Hashimoto, H. Kominami, J. Phys. Chem. C 117 (2013) 16983–16989.
[31] T. Mitsudome, K. Kaneda, Green Chem. 15 (2013) 2636.
[32] D. Ren, L. He, L. Yu, R.-S. Ding, Y.-M. Liu, Y. Cao, H.-Y. He, K.-N. Fan, J. Am. Chem. Soc. 134 (2012) 17592–17598.
[33] M.-C. Daniel, D. Astruc, Chem. Rev. 104 (2004) 293–346.
[34] C. Burda, X. Chen, R. Narayanan, M.A. El-Sayed, Chem. Rev. 105 (2005) 1025–1102.
[35] M.D. Hughes, Y.-J. Xu, P. Jenkins, P. McMorn, P. Landon, D.I. Enache, A.F. Carley, G.A. Attard, G.J. Hutchings, F. King, Nature 437 (2005) 1132.
[36] A. Corma, P. Serna, Science 313 (2006) 332–334.
[37] Y. Xia, Y. Xiong, B. Lim, S.E. Skrabalak, Angew. Chem. Int. Ed. 48 (2009) 60–103.
[38] N. Dimitratos, J.A. Lopez-Sanchez, G.J. Hutchings, Chem. Sci. 3 (2012) 20–44.
[39] M. Conte, H. Miyamura, S. Kobayashi, V. Chechik, J. Am. Chem. Soc. 131 (2009) 7189–7196.
[40] R. Juarez, S.F. Parker, P. Concepcion, A. Corma, H. Garcia, Chem. Sci. 1 (2010) 731–738.
[41] A. Maldotti, A. Molinari, R. Juarez, H. Garcia, Chem. Sci. 2 (2011) 1831–1834.
[42] C.-H. Hao, X.-N. Guo, Y.-T. Pan, S. Chen, Z.-F. Jiao, H. Yang, X.-Y. Guo, J. Am. Chem. Soc. 138 (2016) 9361–9364.

[43] S. Sarina, E. Jaatinen, Q. Xiao, Y.M. Huang, P. Christopher, J.C. Zhao, H.Y. Zhu, J. Phys. Chem. Lett. 8 (2017) 2526–2534.
[44] W. Cui, H. Zhu, M. Jia, W. Ao, Y. Zhang, B. Zhaorigetu, React. Kinet. Mech. Cat. 109 (2013) 551–562.
[45] S. Zhang, Z.-Q. Huang, Y. Ma, W. Gao, J. Li, F. Cao, L. Li, C.-R. Chang, Y. Qu, Nat. Commun. 8 (2017) 15266.
[46] P. Christopher, H. Xin, A. Marimuthu, S. Linic, Nat. Mater. 11 (2012) 1044–1050.
[47] C. Costentin, M. Robert, J.M. Saveant, J. Am. Chem. Soc. 126 (2004) 16051–16057.
[48] Y. Cao, Z. Sui, Y. Zhu, X. Zhou, D. Chen, Acs. Catal. 7 (2017) 7835–7846.
[49] S. Kohtani, E. Yoshioka, K. Saito, A. Kudo, H. Miyabe, J. Phys. Chem. C 116 (2012) 17705–17713.
[50] T.V. Chciuk, W.R. Anderson Jr., R.A. Flowers II, J. Am. Chem. Soc. 138 (2016) 8738–8741.